Single-molecule long-read methylation profiling reveals regional DNA methylation regulated by Elongator Complex Subunit 2 in Arabidopsis roots experiencing spaceflight

Mingqi Zhou[1], Alberto Riva[2], Marie-Pierre L. Gauthier[3], Michael P. Kladde[3], Robert J. Ferl[1,4,*], Anna-Lisa Paul[1,2,*]

[1]Department of Horticultural Sciences, University of Florida, 2550 Hull Road, Fifield Hall, Gainesville FL, 32611, USA

[2]Interdisciplinary Center for Biotechnology Research, University of Florida, 2033 Mowry Road, Gainesville FL, 32610, USA

[3]Department of Biochemistry and Molecular Biology, University of Florida, 2033 Mowry Rd, Gainesville, FL 32608, USA

[4]Office of Research, University of Florida, 1523 Union Rd, Grinter Hall, Gainesville, FL, 32611, USA

*Corresponding authors: robferl@ufl.edu (RJF), alp@ufl.edu (ALP)

Abstract

The Advanced Plant Experiment-04 - Epigenetic Expression (APEX04-EpEx) experiment onboard the International Space Station examined the spaceflight-altered cytosine methylation in two genetic lines of *Arabidopsis thaliana*, wild-type Col-0 and the mutant *elp2-5,* which is deficient in an epigenetic regulator Elongator Complex Subunit 2 (ELP2). Whole-genome bisulfite sequencing (WGBS) revealed distinct spaceflight associated methylation differences, presenting the need to examine specific space-altered methylation at single molecule resolution to associate specific changes over large regions of spaceflight related genes. Therefore flap-enabled next-generation capture (FENGC), a novel targeted multiplexed DNA capture and enrichment technique allowing cleavage at any specified sites, was applied to survey spaceflight-altered DNA

methylation at the single-molecule level. The FENGC capture panel contained 108 targets ranging from 509 to 704 nt within the promoter or gene body regions of gene targets derived from spaceflight whole-genome data sets. In addition to genes with significant changes in expression and average methylation levels between spaceflight and ground control, targets without differentially methylated WGBS but with space-altered distributions of the proportion of methylated cytosines per molecule were further identified. Moreover, trends of co-methylation of different cytosine contexts were exhibited in the same DNA molecules. We further identified significant DNA methylation changes in three previously biological process-unknown genes, and two of them showed enhanced root growth rate in loss-of-function mutants (named as *ELP2-regulated Methylation in Orbit 1* and *2*). FENGC makes multiplexed targeted single-molecule profiling of methylation simple and cost-effective, which provides an additional power to population-based data for methylation analysis and identification of epigenetically modified substrates in plants. This case study has revealed regional spaceflight-altered methylation in selected targets, which were not identified by short-read methods in spaceflight plants. The newly identified *EMO1* and *EMO2* are root growth regulators, which can be epigenetically involved in plant adaptation to spaceflight.

Introduction

DNA methylation epigenetically modulates gene expression and impacts chromatin structure to function in physiological adaptation to environmental changes in eukaryotes (Zhang *et al.*, 2018). Plants will play an important role in the human life support systems envisioned for spaceflight and planetary exploration habitats (Wheeler, 2010; Zabel *et al.*, 2016). Spaceflight presents a unique environmental challenge for plants, an environment that is outside the evolutionary experience of any terrestrial organism. Epigenetic change plays an important role in environmental adaptation, and it is crucial to understand the role of epigenetics in plant adaptation to this novel environment (Paul *et al.*, 2021; Zhou *et al.*, 2019). The Advanced Plant Experiment-04 - Epigenetic Expression (APEX-04) experiment onboard the International Space Station (ISS)

examined the spaceflight-altered cytosine methylation in *Arabidopsis thaliana* (Arabidopsis) using *elp2-5*, a mutant of an epigenetic regulator, Elongator Complex Subunit 2 (ELP2), along with Col-0, a wild-type control (Paul *et al.*, 2021). RNA sequencing (RNAseq) and Whole genome bisulfite sequencing (WGBS) revealed remodeled transcriptomes and DNA methylomes during spaceflight, remodeling that was regulated by ELP2. The spaceflight *elp2-5* phenotype was distinct from the space-grown wild-type plants in that root growth did not present a typical spaceflight directionality, which orients root growth away from the germinating seed, but rather displayed a distinct clumping of roots clustered around the seed. The molecular phenotype exhibited distinct differences in the transcriptome and methylome compare to the ground controls, with a majority of differentially expressed genes in *elp2-5* roots being also differentially methylated between spaceflight samples and ground controls (Paul *et al.*, 2021).

However, the short-read sequencing used in WGBS precludes the ability to phase regional epigenetic signatures along individual molecules such as consecutive methylated cytosines relative to transcription factor binding, nucleosome positioning, histone incorporation and modification (Edwards *et al.*, 2017; Zhang *et al.*, 2018). Moreover, the WGBS detection of differentially methylated cytosines (DmCs) can be affected by sequencing depth and false positives due to overestimation of 5mC level (Feng *et al.*, 2020; NEB), and further downstream analyses including differentially methylated region analysis rely on DmCs (Chen *et al.*, 2016; Kishore and Pelizzola, 2018).

Flap-enabled next-generation capture (FENGC) is a novel, strand-specific DNA capture method that allows DNA methylation analysis with long reads of user-defined target regions (Zhou *et al.*, 2022). FENGC enables sensitive characterization of contiguous single molecules over larger regions, thereby providing a deeper insight into the methylation state than that afforded by the averaged state of methylation obtained by multiple short reads. In addition, compared with WGBS, FENGC increases coverage depth in regions of interest, which improves data quality and minimizes cost of reads in unwanted areas. Furthermore, FENGC has advantages of liberty in target region

selection and cost-effectiveness that are superior to other targeted-sequencing methods. First, the formation of flap structure on DNA strands of target regions using user-designed oligos and cleavage by flap endonuclease avoid the limits due to sequence dependence of enzymes for target selection. For DNA methylation survey, the target capture of FENGC occurs prior to deamination of 5mC, also avoiding the primer design limits of regular methyl-PCR due to potentially methylated sites. Second, the utilization of standard oligos for targeting without modified bases as well as the single-tube experimental protocol significantly lower the cost (Kladde *et al.*, 2022; Zhou *et al.*, 2022). Hence, this tool is ideal for targeting customer-designed specific panels especially for DNA methylation analysis of plants possessing 5-methylation in three types of cytosine context, CG/CHG/CHH (Grimanelli and Ingouff, 2020). The accuracy and efficiency of enzymatic methyl-seq, which is part of the FENGC procedure, has been verified in plants (Feng *et al.*, 2020); however, FENGC has yet to be applied to methylation analysis in plants.

Therefore, we set out to demonstrate the effective application of FENGC in plant methylation contexts. The observed phenotypical and molecular alteration in roots of Col-0 and *elp2-5* grown on the ISS in APEX-04 present a short-read methylation dataset for a comparison with methylation profiles assayed by FENGC single-molecule long reads. WGBS-unidentified differential modification of DNA methylation substrates in functionally-annotated genes as well as unknown genes of plants grown in orbit have been detected.

Results and discussion

Quality of FENGC assay

In the FENGC assay, strand cleavage was directed by precise targeting of FEN1 on flap formation, which was user-defined through oligo design so that sequence-based limits, such as reliance on restriction sites or specific motif sequences, could be avoided. The target panel for capture and assay contained 108 genic regions ranging from 509 to 704 nt (Table S1), with mean of 580 nt and median of 572 nt, within the promoter or gene

body regions of 87 epigenetically regulated genes derived from our APEX-04 spaceflight and related experiments (Paul *et al.*, 2021, 2013; Paul, Zhou, *et al.*, 2017; Zhou *et al.*, 2019). This design therefore provides strand specific methylation data over the entire range of the targeted sequences.

The capture was performed as a single-tube multiplex reaction followed by enzymatic methyl-PCR (oligos are listed in Table S2). The FENGC products were subjected to PacBio long-read HiFi sequencing. For APEX04 samples, including Ground control Col-0 Roots (GCR), Flight Col-0 Roots (FCR), Ground control elp2-5 Roots (GER) and Flight elp2-5 Roots (FER), capture products consistently yielded around 90% reads on-target ratio and, on average, 82% targets were detected by at least 10 reads after filtering and combining the four biological replicates from each sample (Figure 1A and 1B; Table S3). The GC content of the 108 targets, ranging from 19% to 52%, was positively correlated with the aligned reads number (Figure 1C; Figure S1), whereas there was a modest negative correlation in FENGC targets with an average GC content above 50% (Zhou *et al.*, 2022). This indicates that both high and low GC content of targets influenced the reads yield of FENGC products.

Targeted DNA capture and sequencing analyses have been widely deployed in plant genomic studies (Ostezan *et al.*, 2021). For invitro targeted assay in plant genomes, FENGC possesses multiple advantages compared with other methods, including high liberty for customer design, high performance in sequencing depth, target number, on-target ratio, and low cost (Table 1). Especially for targeted DNA methylation detection in plants, to date, only singleplexed or multiplexed bisulfite-PCR has been regularly used, which suffers from the limits in sequencing read length, primer region selection, and assay capability. To our knowledge, FENGC provides the unique opportunity for plant research community for multiplexed, targeted sequencing analysis on DNA methylation.

Regional methylation detection by FENGC in comparison with WGBS data

One major advantage of single-molecule profiling of DNA methylation is that the contiguous long reads allow assessment of every cytosine within same DNA molecule,

thereby presenting a coherent regional methylation status of that entire gene element within a cell. In addition, the average methylation levels in cytosines across all molecules can be derived from the data for comparison to WGBS data. For the present study, long-read, single-molecule sequencing identified gene targets showing both significant differential expression and average methylation level changes between spaceflight and ground control. Moreover, space-altered distributions of the proportion of methylated cytosines per molecule were further revealed.

Combining the four biological replicates, GCR, FCR, GER and FER yielded 79, 93, 88 and 96 target regions with coverage of at least 10 reads (Table S3; Table S4). The distributions of the proportion of methylated cytosines per molecule in each target region were calculated. Among them, 12 targets in 12 genes showed differential methylation proportion per molecule (DmPPM) for the comparison between spaceflight and ground control in Col-0 or *elp2-5* (Table S1). Meanwhile, the APEX04 WGBS-identified DmCs (methylation difference > 0.2, FDR < 0.01) between spaceflight and ground control were examined within 108 target regions of FENGC. Col-0 and *elp2-5* showed 8/2/7 and 5/2/2 targets possessing DmPPM for CG/CHG/CHH methylation, respectively. Among these regions, only one target with DmCHH for Col-0 and two targets with DmCHG for *elp2-5* were identified by WGBS (Table S1). The comparison of detection in DmPPM and DmC demonstrated that the changes of contiguous methylation status observable in a specific subpopulation of molecules in FENGC may be indiscernible in a population-based analysis.

Next, we present four examples associated with defense responses to stimuli and three biological process-unknown genes regulated by ELP2 during plant growth in spaceflight to exhibit details of space-altered methylation status that are newly uncovered by FENGC (Table S1). Considering these seven targets, the methylation levels of cytosines exhibited correlation coefficients above 0.93 between any two biological replicates and above 0.95 between FENGC and WGBS results (Figure 1D). In each region, 93%-100% of the mapped reads are full-length, containing all CG/CHG/CHH sites of each target region (Figure S2). These results verify the high data quality for captured targets in the FENGC assay of space plants.

Identification of previously unidentified space-altered DNA methylation in defense-related gene targets

Among 12 genes exhibiting DmPPM of spaceflight vs ground control, four defense-related genes showed space-triggered DNA methylation modification that was not discernible in WGBS. The first three examples were examined with CG methylation, for which DmPPM was shown in CG sites but no DmCG (methylation difference > 0.2, FDR < 0.01) between spaceflight and ground control was detected by WGBS in these target regions. *CML46* (AT5G39670), a gene encoding a calmodulin-like protein showing significant transcriptional down-regulation during spaceflight in Col-0 but not *elp2-5* plants, was assayed in a promoter region containing a MYB-like DNA binding element (Figure 2A and 2B). Flight and ground control Col-0 roots (FCR and GCR), but not roots from *elp2-5* (FER and GER), showed a significant difference in the CG methylation level in an area flanking the MYB-like element, which contained five CG sites (Figure 2C, in dashed frame). Consistent with these data, CG methylation proportion per molecule (mPPM) in this target region was significantly higher in FCR than GCR (Figure 2D). A significant difference between GCR and GER was also observed. FENGC showed more molecules containing consecutively methylated CG sites in FCR (12%) compared to GCR (6.9%) in the area flanking this *cis*-regulatory element (Figure 2E). Consistency between the levels of gene transcription, WGBS-derived population-based methylation status, and FENGC-derived mPPM, support the biological conclusion that ELP2 played a negative role in expression and a positive role in promoter methylation of *CML46* in spaceflight.

ABCB17 (AT3G28380), an ATP-binding cassette transporter gene that also showed a significantly lower transcription level in FCR than GCR, was assayed in a gene body region (Figure S3A and S3B). The overall patterns of averaged regional CG methylation levels were very similar between the four samples, which did not show significant changes between any pair of samples (Figure S3C); however, the CG mPPM in this target region was significantly higher in FCR than in GCR (Figure S3D). The FENGC single-molecule data showed that 3.7% of the reads in FCR possessed at least 6

consecutive methylated CG sites, whereas in GCR the percentage was 0.8% (Figure S3E). Biologically, *ABCB17* was repressed by spaceflight and ELP2 contributed to its transcription and gene body methylation.

Similarly, in the promoter region of *DEFL* (AT4G22217), a defensin-like gene (Figure S4A and S4B), the patterns of averaged CG methylation levels were highly similar and no significant alterations were detected between any two samples (Figure S4C); however, CG mPPM was significantly higher in FER than GER (Figure S4D and S4E). This higher methylation proportion correlates with the lower transcription level of this gene in FER compared to GER (Figure S4B). ELP2 enhanced expression and repressed promoter methylation of *DEFL* in spaceflight. These examples suggest that long-read FENGC single-molecule level methylation profiling can be more revealing of consequential methylation changes compared with population-based methylation methods such as WGBS, especially when alterations potentially occur in a subpopulation of cells within a sample.

For the fourth example, a promoter fragment containing a MeJA-responsive element was selected in *PDF1.1* (AT1G75830), a gene coding a pathogenesis-related protein belonging to the plant defensin family and showing a significant spaceflight induction in *elp2-5* (Figure 3A and 3B). The average methylation level per site over all sequenced molecules showed significant differences at CHG and CHH sites between GER and GCR, as well as in CHH sites between FCR and GCR (Figure 3C). For mPPM, significant differences were detected in all pairwise comparisons between flight conditions and genotypes at cytosines in all three methylation contexts (Figure 3D). DmCs of WGBS between GER and GCR correlated with methylation changes detected by FENGC (Figure 3D; Table S1), while between spaceflight and ground control only three DmCGs in *elp2-5* were identified by WGBS, and the FENGC determined methylation level changes were smaller than 0.2 at these three sites (Figure 3C), which was in line with the WGBS overestimation of methylation level compared with EM-seq, especially in CHG sites (Feng *et al.*, 2020). The patterns of methylation proportion in DNA molecules demonstrated that three cytosine contexts showed a trend of co-methylation in this region among cells in the population (Figure S5). Within each

molecule, methylation proportion of CG is higher than CHG in 97.9% reads, and that of CHG is higher than CHH in 87.5% reads (Figure 4A). Although three types of cytosine methylation exhibited a trend of coordination in the whole cell population, they could spread independently within subpopulations of cells. The CG methylation proportions were above 0.57 in all reads of GCR and above 0.28 in GER, while FCR and FER had reads with CG methylation proportion as low as 0. These data indicate that more molecules were hypomethylated in this region in *elp2-5* compared with Col-0 and in spaceflight compared with ground control.

The profiling of methylation data in this example also showcases another advantage of long-read, single-molecule FENGC assay of DNA methylation in plants, which is that all three methylation sequence contexts (CG/CHG/CHH) can be identified and plotted for the same molecule, thereby examining the entire methylation status of a gene region. To determine the spatial distribution of these methylation differences, three separate but correlated panels were plotted for CG, CHG and CHH methylation in the same DNA molecule per row (Figure 3E). In these plots, black areas are unmethylated regions, red areas are methylated regions, and gray areas are transition zones between methylated and unmethylated sites. It is visually apparent that spaceflight results in more unmethylated regions in Col-0, with the deepest loss of methylation concentrated near the MeJA-responsive element. It is also visually apparent that *elp2-5* shows a deeper loss of methylation in that region. For the CG methylation context, a footprint showing consecutive non-methylation of the first 2 CG sites in flanking area of the MeJA-responsive element was identified in 8.4%, 18.0%, 39.4% and 44.0% reads in GCR, FCR, GER and FER, respectively, quantifying the loss of CG methylation in this area. Interestingly, 60%, 86.5%, 97.5% and 97.6% reads with consecutive non-methylation in the second and the third CG sites in GCR, FCR, GER and FER, respectively, were also included in this footprint and showed consecutive non-methylation of the first 3 CG sites. In addition, CHG and CHH methylation proportions were significantly lower in the footprint area in the reads containing this footprint (Figure 4B). These results are consistent with the previously observed high frequency of co-methylation/demethylation in nearby cytosines in Arabidopsis (Tran *et al.*, 2018), and demonstrate that FENGC

provides further opportunities for studying all three types of co-methylation methylation along each single molecule .

Four targets shown here are associated with plant defense signaling, which is largely utilized in spaceflight adaptation of plants and the related genes can be involved in regulation of root growth phenotypes during spaceflight (Califar *et al.*, 2020; Paul, Sng, *et al.*, 2017). It has also been reported that ELP2 modulates the epigenetic control of plant immune responses and defense processes (Wang *et al.*, 2013). The newly identified space-altered methylation in these targets is involved in ELP2-regulated defense/immunity-related pathways that may function in adaptation of plant roots grown in orbit.

Identification of novel spaceflight-related epigenetic modification in biological process-unknown genes

The 12 genes with DmPPM between spaceflight and ground control were annotated using the Database for Annotation, Visualization and Integrated Discovery (DAVID, https://david.ncifcrf.gov/). Three genes were returned without gene ontology (GO) or functional annotation for biological process. Further investigation verified that the three target regions within these three genes possessed significant alteration between spaceflight and ground control in both average cytosine methylation level as well as mPPM in Col-0 or *elp2-5*. Moreover, loss-of-function mutants of two of these genes showed a root growth phenotype. We dubbed the two genes that could be epigenetically involved in plant adaptation to spaceflight under regulation of ELP2, AT1G27565 and AT5G52710, as *ELP2-regulated Methylation in Orbit* (*EMO*) *1* and *2*, respectively.

A promoter region was captured by FENGC for *EMO1* (AT1G27565), containing an anaerobic-responsive element (ARE) beside the transcription start site (TSS) (Figure 5A). The presence of the ARE is consistent with the observed induction of hypoxia-responsive genes in spaceflight transcriptome data sets (Choi *et al.*, 2019; Zhou *et al.*, 2019). *EMO1* was significantly up-regulated by spaceflight in *elp2-5*, but not in Col-0

(Figure 5B). Regional average methylation level analysis detected significant differences between genotypes and between spaceflight and ground control in Col-0 only for CG sites (Figure 5C). The calculation of mPPM showed significant alteration between spaceflight and ground control in all three types of cytosine context for Col-0 and in CG sites for *elp2-5* (Figure 5D). Visualization of three types of methylated cytosines in each single molecule revealed footprints of methylation-free areas in areas in subpopulations of epialleles (Figure 5E). Significantly, more molecules in *elp2-5* lacked cytosine methylation within this region than Col-0, and more molecules with methylation-free areas beside TSS were identified in spaceflight samples than ground control. These results were consistent with the observation of lower correlation of mPPM between GG and CHH in GCR than other samples (Figure S6 and S7). After demethylation initiated by spaceflight or mutation of ELP2 in a small proportion of cells, the co-methylation for different types of cytosine context in those molecules had been changed accordingly. Overall, ELP2 played a negative role in *EMO1* expression and maintained cytosine methylation of the *EMO1* promoter in a subpopulation of cells in roots. Spaceflight promoted demethylation in flanking areas of *EMO1* TSS, while the induction of *EMO1* transcription in space was repressed by ELP2.

The *EMO2* (AT5G52710) gene belongs to copper transport protein family (de Abreu-Neto *et al.*, 2013). The captured promoter region contains two MeJA-responsive elements (Figure 6A). The transcription level of *EMO2* was lower in *elp2-5* than Col-0, and lower in spaceflight than ground control (Figure 6B). Accordingly, the regional average methylation levels were significantly higher in *elp2-5* than Col-0 for CG and CHG sites, which was consistent with DmC analysis of WGBS (Figure 6C). In contrast, CHH differential methylation levels detected by FENGC were smaller than that of WGBS. The mPPMs were higher in spaceflight than ground control in all three cytosine types for *elp2-5*, which explained the space-repressed expression of *EMO2* when ELP2 was deficient (Figure 6B and 6D). Intriguingly, the areas of two MeJA-responsive elements both harbored a footprint of low CG methylation, whereas CHG sites localized within these elements showed methylation peaks, especially in *elp2-5* (Figure 6C and 6E). When ELP2 was inactivated, the two CG methylation footprints were largely lost. Moreover, the correlations of mPPM between different types of cytosine context were

lower in *elp2-5* than Col-0 (Figure S8 and S9). These results indicate the role of ELP2 in the maintenance of hypomethylated motifs and coordination of methylation for different cytosine types in this chromatin region, which could contribute to activation of *EMO2* transcription.

The AT4G04990 gene encodes a serine/arginine repetitive matrix-like protein and the transcripts can be transported between roots and shoots (Thieme *et al.*, 2015). The captured promoter region contains a TC-rich repeat that is related to defense and stress responses (Figure S10A). The transcription level of AT4G04990 was down-regulated by both spaceflight and mutation of ELP2 (Figure S10B). No DmC in WGBS or significant difference of average methylation level in FENGC was identified for this region, while DmPPMs of CG and CHH were detected between spaceflight and ground control in Col-0 (Figure S10C and S10D). In this region, a stronger correlation was observed between mPPMs of CHG and CHH than that of CG and CHH (Figure S10E; Figure S10 and S11). Correlation between mPPMs of CG and CHG increased by spaceflight in Col-0 (Figure S11), which was partially due to space-induced demethylation of CG sites in a subpopulation of cells (Figure S10D and S10E; Figure S12). The coordination of CG and non-CG methylation might be related to the transcription repression of AT4G04990 in spaceflight and *elp2-5*.

The features in alteration of DNA methylation at the single molecule level, such as DmPPM and methylation footprints, would be more informative for detection of epigenetic changes and better connect the regulation of gene expression to epigenetic modification, compared with population-based DmC levels that would lose epigenetic information in the single molecules. Therefore, FENGC data provide additional clues for further selection of target genes of interest for downstream analysis, especially when candidates include unknown genes.

***EMO1* and *EMO2* are negative regulators of root growth**

T-DNA insertion lines of the three biological process-unknown genes identified by FENGC were characterized. Two lines of each gene tested showed disrupted gene

expression levels compared with Col-0 (Figure S13). Thus, SALK_092504 and SAIL_344_F07 were named as *emo1-1* and *emo1-2*, while SALK_140748C and SALK_091636C were named as *emo2-1* and *emo2-2*, respectively. In a constant LED light condition that was similar with Veggie facility onboard ISS, *emo1* and *emo2* mutants showed significantly enhanced root growth rates compared with Col-0 (Figure 7A-C). The primary root length of *emo1-1*, *emo1-2*, *emo2-1*, and *emo2-2* were significantly longer than that of Col-0 in 4-day and 7-day old seedlings. The two mutants of AT4G04990 exhibited similar growth phenotype with wild type. Meanwhile, treatments using 2-D clinorotation at 4 rpm or reorientation to 90˚ did not show altered gravitropic responses in roots of any line tested, although roots of *EMO1* and *EMO2* mutants still grew faster than Col-0 on the clinostat (Figure S14 and S15). These results demonstrated that *EMO1* and *EMO2* are two negative regulators of root growth, but not regulators of root gravitropism.

Remodeled plant root growth has been reported in orbital spaceflight (Paul *et al.*, 2012). Both direction of root tips during growth and the growth rate of roots were impacted in Arabidopsis plants grown on the ISS (Kwon *et al.*, 2015; Paul *et al.*, 2012; Paul, Sng, *et al.*, 2017). The primary root length of 8.5-day old seedlings for both Col-0 and Ws were significantly shorter in flight samples than ground control. This influence on root growth from spaceflight involves epigenetic and transcriptional modulation (Paul *et al.*, 2021, 2013). As a epigenetic modulator of root growth and development, ELP2 modifies DNA methylation or histone acetylation of a range of transcription factors and other developmental regulators in roots (Jia *et al.*, 2015). On the ISS, the *elp2-5* mutant exhibited severe growth retardation in roots compared with Col-0 (Paul *et al.*, 2021). Here, *EMO1* and *EMO2* have been identified as two downstream targets of DNA methylation modification led by ELP2 and/or caused by extraterritorial environment. Together with the root growth rate phenotype in their mutants, *EMO1* and *EMO2* can play a role in root growth regulation during space adaptation of plants, which may involve the epigenetic signaling pathways controlled by ELP2. Moreover, although the mutants of AT4G04990 did not show root growth alteration on the ground, further investigation will be needed to examine its function in space.

Conclusion

Whereas short-read WGBS only detects alteration of average methylation level in cytosines, targeted long-read, single-molecule profiling reveals the detailed epigenetic modifications occurring in cell subpopulations and identifies epialleles present at low frequencies. On one hand, FENGC and WGBS show consistency in the detection of cytosine methylation levels. On the other hand, FENGC enables single-molecule determination of methylation alteration, which greatly extends interpretation beyond that of WGBS. Analysis of DmPPM serves as critical addition to DmC data in methylation survey. The capacity of target cleavage at any specified sites enables wide application of FENGC, such as studies on plant development, environmental responses, and generation of biomarkers. In the current work, FENGC allowed us to survey genic regions of interest from primary transcriptomic and WGBS screening, successfully identifying two novel root growth regulators through analysis of DNA methylation alteration. In summary, FENGC provides the plant and space biology communities with a powerful tool for the practical application of multiplexed targeted sequencing and coordinated methylation analysis at single-molecule level as routine experiments. This FENGC screen of spaceflight-associated genes revealed candidate genes with regulatory regions that harbored significant alterations in consecutive spans of methylation. Further genetic analysis identified *EMO1* and *EMO2*, which are novel candidates for further investigation of root growth regulatory signaling elicited by ELP2 in plant adaptation to spaceflight.

Materials and methods

Plant materials and operations of spaceflight and ground controls

The *Arabidopsis thaliana* lines Col-0 and *elp2-5*, as well as spaceflight experimental operations, have been previously documented (Paul *et al.*, 2021; Wang *et al.*, 2013). The Advanced Plant Experiment 04 – Epigenetic Expression (APEX-04-EPEX) spaceflight experiment was launched onto International Space Station (ISS) through the

SpaceX mission CRS-10. In brief, seeds were sterilized and sown on growth medium containing 0.5% phytagel, 0.5× Murashige–Skoog salts, 0.5% (w/v) sucrose, and 1 × Gamborg's Vitamin Mixture, in Petri dishes (100 mm × 15 mm; Fisher Scientific, Pittsburgh, USA), which were then sealed with breathable tape (3M Micropore, Maplewood, USA). Plants were grown in the Vegetable Production System (Veggie) facility on the ISS and the Veggie hardware in the ISS environmental simulator (ISSES) chamber at Kennedy Space Center under constant LED light of 100–135 μmol/m^{2}s Photosynthetically Active Radiation (PAR) until 11 days after germination, prior to harvest using RNAlater (Ambion, Grand Island, USA) in Kennedy Space Center fixation tubes (KFTs). Plants from each plate were collected into individual KFTs and stored at -80°C until delivery to the lab for analysis.

Genomic DNA Isolation and flap-enabled next-generation capture (FENGC) assay

DNA extraction was conducted using the protocol designed for RNAlater preserved plant samples (LeFrois *et al.*, 2016). The same set of DNA samples from Col-0 and *elp2-5* root tissues used for whole-genome bisulfite sequencing (WGBS) (Paul *et al.*, 2021) were subjected to flap-enabled next-generation capture (FENGC) assay. The samples included four biological replicates of each condition: Ground control Col-0 Roots (GCR), Flight Col-0 Roots (FCR), Ground control *elp2-5* Roots (GER) and Flight *elp2-5* Roots (FER).

FENGC oligo-1, -2 and -3 were designed using FENGC Oligonucleotide Designer (FOLD) program (https://github.com/uf-icbr-bioinformatics/FOLD), to bind target DNA to form 5′ flap structures that were cleaved by flap endonuclease (FEN), which enabled ligation between target fragments and universal adaptors (Zhou *et al.*, 2022). There were 108 targets selected within promoter and gene body regions of 87 genes of interest derived from previous spaceflight-associated transcriptome and DNA methylome studies (Paul *et al.*, 2021, 2013; Paul, Zhou, *et al.*, 2017; Zhou *et al.*, 2019). The detailed information of the 108 targets is in Table S1. All oligos used in this study are listed in Table S2. All captured sequences are from the coding strand of each gene.

FENGC experiments were performed as described by Kladde and colleagues (Zhou *et al.*, 2022), with minor modifications. In brief, approximately 200 ng of Arabidopsis genomic DNA was fragmented by sonication using a Bioruptor Pico (Diagenode, Denville, USA) for 6 cycles of 5 sec on and 30 sec off in 20 µl ddH_2O. The concentration of oligo-1, -2, and -3 was 18 nM each in the master tube as recommended (Zhou *et al.*, 2022). Flap cleavage was performed in the presence of FENGC universal oligo 1-T (U1-T oligo), flap oligos-1 and -2 specific for 108 targets, and thermostable FEN1 (New England Biolabs, Ipswich, USA). Ligation was initiated by adding a stock mixture of oligos-3 for all 108 targets, U2 oligo, and Ampligase (Lucigen, Middleton, USA) to the same tube. DNA not ligated to U2 oligo and therefore not protected by 3' C3 Spacer was removed by addition of exonucleases I and III (NEB, Ipswich, USA). The enriched products were purified and then subjected to enzymatic methylation conversion according to the manual of NEBNext Enzymatic Methyl-seq Conversion Module (NEB, Ipswich, USA). Converted DNA was amplified for 23 cycles using U1 and U2 primers and KAPA HiFi HotStart Uracil+ DNA polymerase (Roche, Pleasanton, USA), according to the manufacturer's instructions. FENGC amplification products were purified and product quality and quantity were determined using Agilent TapeStation D1000 system (Agilent, Santa Clara, USA) and Qubit 3 Fluorometer (Thermo Fisher, Waltham, USA), respectively.

Pacific Biosciences Sequel IIe SMRT sequencing and data analysis

The library construction and sequencing of FENGC products on the Pacific Biosciences (PacBio) Sequel IIe SMRT platform was performed by Interdisciplinary Center for Biotechnology Research (ICBR) at the University of Florida. The HiFi reads were generated using 30-h movie of circular consensus (CCS) mode with filtering for ≥3 passes per single polymerase read, with default settings for other parameters. HiFi reads mapping and visualization of DNA methylation states of single molecules were performed using MethylMapper as previously described (Nabilsi *et al.*, 2014), with modifications to accommodate plant genomes. Reads with more than three consecutive methylated CHH sites were removed (Liu *et al.*, 2021).

Demultiplexed CCS reads data files of PacBio Sequel IIe SMRT sequencing have been deposited with the accession number of PRJNA857037 to BioProject database (https://www.ncbi.nlm.nih.gov/bioproject/) in National Center for Biotechnology Information (NCBI), and with the OSD identifier of OSD-625 (DOI: 10.26030/rp5n-0d70) in NASA GeneLab.

Roots characterization assay

The *Arabidopsis thaliana* T-DNA insertion lines SALK_092504 (*emo1-1*), SAIL_344_F07 (*emo1-2*), SALK_140748C (*emo2-1*), SALK_091636C (*emo2-2*), SAIL_205_A08, and WiscDsLox441G3 were obtained from Arabidopsis Biological Resource Center (https://abrc.osu.edu/). Seeds were sterilized, incubated in ddH_2O at 4°C for 3 days, and then sown on 0.5x Murashige–Skoog medium in Petri dishes as described above. Plates were placed on vertical racks at 21°C in 24 h LED light condition at approximately 100 μmol/m^2s PAR. The 4-day old were photographed. Then plants were subjected to three treatments. The first set of plates were kept quiescent and seedlings were grown to 7-day old and photographed. The second set of plates were mounted to a 2-dimentional clinostat to be rotated at 4 rounds per min until plants were 7-day old, and then photographed. The third set of plates were reoriented 90° to the horizontal, and photographed at 0 h, 6 h and 24 h after reorientation. Roots were traced and measured using JFilament plugin of ImageJ (Li *et al.*, 2009; Smith *et al.*, 2010). Root growth measurements were processed using the R script RootMeasurement (https://github.com/eschultzphd/RootMeasurement/tree/master) (Schultz *et al.*, 2017). The quantitative real-time PCR (qPCR) assay to verify gene knock-out or knock-down was performed using roots of 7-day old seedlings as previously described (Zhou *et al.*, 2017). UBQ11 (AT4G05050) was used as the internal control and primers are listed in Table S2.

FENGC materials availability

Requests for a detailed FENGC protocol and updated versions of FOLD should be directed to Michael Kladde (kladde@ufl.edu).

Funding

This work was supported by NASA grants NNX14AT24G and 80NSSC19K0130 to A-LP and RJF. Development of FENGC was supported by Defense Threat Reduction Agency grant HDTRA1-16-1-0048 awarded to MPK as a co-PI and NIH grant R01 CA155390 awarded to MPK.

Acknowledgments

We thank members of UF Space Plants Lab for helpful discussion and assistance in experiments, as well as members of UF ICBR, NextGen DNA sequencing (RRID:SCR_019152), Bioinformatics (RRID:SCR_019120) and Gene Expression and Genotyping (RRID:SCR_019145) cores, for their support and services. We also thank Jason O. Brant for his assistance in developing the FOLD program.

Conflict of interest

A United States patent application (#18/551,004) was filed on September 18, 2023, and is pending. M.Z. and M.P.K. are two of the co-inventors.

Author contributions

MZ, RJF and A-LP designed this study. MZ conducted the experiments and analyzed the data. MZ and MPK developed the FENGC methodology. AR, M-PLG and MPK contributed to the FENGC oligo design program. MZ, MPK, RJF and A-LP wrote the manuscript.

Data availability

Demultiplexed CCS reads data files of PacBio Sequel IIe SMRT sequencing have been deposited with the accession number of PRJNA857037 to BioProject database (https://www.ncbi.nlm.nih.gov/bioproject/) in National Center for Biotechnology Information (NCBI), and with the OSD identifier of OSD-625 (DOI: 10.26030/rp5n-0d70) in NASA GeneLab.

References

de Abreu-Neto, J.B., Turchetto-Zolet, A.C., de Oliveira, L.F.V., Bodanese Zanettini, M.H., and Margis-Pinheiro, M. (2013) *Heavy metal-associated isoprenylated plant protein (HIPP): characterization of a family of proteins exclusive to plants*. *The FEBS Journal*, **280**, 1604–1616.

Califar, B., Sng, N.J., Zupanska, A., Paul, A.-L., and Ferl, R.J. (2020) *Root Skewing-Associated Genes Impact the Spaceflight Response of Arabidopsis thaliana*. *Frontiers in Plant Science*, **11**.

Chen, D.-P., Lin, Y.-C., and Fann, C.S.J. (2016) *Methods for identifying differentially methylated regions for sequence- and array-based data*. *Briefings in Functional Genomics*, **15**, 485–490.

Choi, W.-G., Barker, R.J., Kim, S.-H., Swanson, S.J., and Gilroy, S. (2019) *Variation in the transcriptome of different ecotypes of Arabidopsis thaliana reveals signatures of oxidative stress in plant responses to spaceflight*. *American Journal of Botany*, **106**, 123–136.

Edwards, J.R., Yarychkivska, O., Boulard, M., and Bestor, T.H. (2017) *DNA methylation and DNA methyltransferases*. *Epigenetics Chromatin*, **10**, 23.

Feng, S., Zhong, Z., Wang, M., and Jacobsen, S.E. (2020) *Efficient and accurate determination of genome-wide DNA methylation patterns in Arabidopsis thaliana with enzymatic methyl sequencing*. *Epigenetics & Chromatin*, **13**, 42.

Giolai, M., Paajanen, P., Verweij, W., Witek, K., Jones, J.D.G., and Clark, M.D. (2017) *Comparative analysis of targeted long read sequencing approaches for characterization of a plant's immune receptor repertoire*. *BMC Genomics*, **18**, 564.

Grimanelli, D. and Ingouff, M. (2020) *DNA Methylation Readers in Plants*. *Journal of Molecular Biology*, **432**, 1706–1717.

Hill, C.B., Wong, D., Tibbits, J., Forrest, K., Hayden, M., Zhang, X.-Q., et al. (2019) *Targeted enrichment by solution-based hybrid capture to identify genetic sequence variants in barley*. *Sci Data*, **6**, 12.

Jia, Y., Tian, H., Li, H., Yu, Q., Wang, L., Friml, J., and Ding, Z. (2015) *The Arabidopsis thaliana elongator complex subunit 2 epigenetically affects root development*. *Journal of Experimental Botany*, **66**, 4631–4642.

Kishore, K. and Pelizzola, M. (2018) *Identification of Differentially Methylated Regions in the Genome of Arabidopsis thaliana*. In: *Plant Chromatin Dynamics: Methods and Protocols* Methods in Molecular Biology (Bemer,M. and Baroux,C., eds) , pp. 61–69. New York, NY: Springer.

Kladde, M.P., ZHOU, M., and NABILSI, N.H. (2022) *Methods and kits for targeted cleavage and enrichment of nucleic acids for high-throughput analyses of user-defined genomic regions*.

Kwon, T., Sparks, J.A., Nakashima, J., Allen, S.N., Tang, Y., and Blancaflor, E.B. (2015) *Transcriptional response of Arabidopsis seedlings during spaceflight reveals peroxidase and cell wall remodeling genes associated with root hair development*. *American Journal of Botany*, **102**, 21–35.

LeFrois, C.E., Zhou, M., Amador, D.M., Sng, N., Paul, A.-L., and Ferl, R.J. (2016) *Enabling the Spaceflight Methylome: DNA Isolated from Plant Tissues Preserved in RNAlater Is Suitable for Bisulfite PCR Assay of Genome Methylation*. *Gravitational and Space Research*, **4**, 28–37.

Li, H., Shen, T., Smith, M.B., Fujiwara, I., Vavylonis, D., and Huang, X. (2009) *Automated actin filament segmentation, tracking and tip elongation measurements based on open active contour models*. In: *2009 IEEE International Symposium on Biomedical Imaging: From Nano to Macro* , pp. 1302–1305.

Liu, W., Gallego-Bartolomé, J., Zhou, Y., Zhong, Z., Wang, M., Wongpalee, S.P., et al. (2021) *Ectopic targeting of CG DNA methylation in Arabidopsis with the bacterial SssI methyltransferase*. *Nat Commun*, **12**, 3130.

López-Girona, E., Davy, M.W., Albert, N.W., Hilario, E., Smart, M.E.M., Kirk, C., et al. (2020) *CRISPR-Cas9 enrichment and long read sequencing for fine mapping in plants*. *Plant Methods*, **16**, 121.

Nabilsi, N.H., Deleyrolle, L.P., Darst, R.P., Riva, A., Reynolds, B.A., and Kladde, M.P. (2014) *Multiplex mapping of chromatin accessibility and DNA methylation within targeted single molecules identifies epigenetic heterogeneity in neural stem cells and glioblastoma*. *Genome Res*, **24**, 329–339.

NEB *NEBNext® Enzymatic Methyl-seq (EM-seq™)*.

Onda, Y., Takahagi, K., Shimizu, M., Inoue, K., and Mochida, K. (2018) *Multiplex PCR Targeted Amplicon Sequencing (MTA-Seq): Simple, Flexible, and Versatile SNP Genotyping by Highly Multiplexed PCR Amplicon Sequencing*. *Frontiers in Plant Science*, **9**.

Ostezan, A., McDonald, S.C., Tran, D.T., Souza, R.S.E., and Li, Z. (2021) *Target region sequencing and applications in plants*. *J. Crop Sci. Biotechnol.*, **24**, 13–26.

Paul, A.-L., Amalfitano, C.E., and Ferl, R.J. (2012) *Plant growth strategies are remodeled by spaceflight*. *BMC Plant Biology*, **12**, 232.

Paul, A.-L., Haveman, N., Califar, B., and Ferl, R.J. (2021) *Epigenomic Regulators Elongator Complex Subunit 2 and Methyltransferase 1 Differentially Condition the Spaceflight Response in Arabidopsis*. *Frontiers in Plant Science*, **12**.

Paul, A.-L., Sng, N.J., Zupanska, A.K., Krishnamurthy, A., Schultz, E.R., and Ferl, R.J. (2017) *Genetic dissection of the Arabidopsis spaceflight transcriptome: Are some responses dispensable for the physiological adaptation of plants to spaceflight?* *PLOS ONE*, **12**, e0180186.

Paul, A.-L., Zhou, M., Callaham, J.B., Reyes, M., Stasiak, M., Riva, A., et al. (2017) *Patterns of Arabidopsis gene expression in the face of hypobaric stress*. *AoB PLANTS*, **9**, plx030.

Paul, A.-L., Zupanska, A.K., Schultz, E.R., and Ferl, R.J. (2013) *Organ-specific remodeling of the Arabidopsis transcriptome in response to spaceflight*. *BMC Plant Biology*, **13**, 112.

Schultz, E.R., Zupanska, A.K., Sng, N.J., Paul, A.-L., and Ferl, R.J. (2017) *Skewing in Arabidopsis roots involves disparate environmental signaling pathways*. *BMC Plant Biology*, **17**, 31.

Smith, M.B., Li, H., Shen, T., Huang, X., Yusuf, E., and Vavylonis, D. (2010) *Segmentation and tracking of cytoskeletal filaments using open active contours*. *Cytoskeleton*, **67**, 693–705.

Thieme, C.J., Rojas-Triana, M., Stecyk, E., Schudoma, C., Zhang, W., Yang, L., et al. (2015) *Endogenous Arabidopsis messenger RNAs transported to distant tissues*. *Nature Plants*, **1**, 1–9.

Tran, H., Zhu, H., Wu, X., Kim, G., Clarke, C.R., Larose, H., et al. (2018) *Identification of Differentially Methylated Sites with Weak Methylation Effects*. *Genes*, **9**, 75.

Wang, Y., An, C., Zhang, X., Yao, J., Zhang, Y., Sun, Y., et al. (2013) *The Arabidopsis elongator complex subunit2 epigenetically regulates plant immune responses*. *Plant Cell*, **25**, 762–776.

Wheeler, R.M. (2010) *Plants for human life support in space: from Myers to Mars*. *Gravitational and Space Biology*, **23**, 25–36.

Zabel, P., Bamsey, M., Schubert, D., and Tajmar, M. (2016) *Review and analysis of over 40 years of space plant growth systems*. *Life Sciences in Space Research*, **10**, 1–16.

Zhang, H., Lang, Z., and Zhu, J.-K. (2018) *Dynamics and function of DNA methylation in plants*. *Nat Rev Mol Cell Biol*, **19**, 489–506.

Zhou, M., Nabilsi, N.H., Wang, A., Gauthier, M.-P.L., Murray, K.O., Azari, H., et al. (2022) *Flap-enabled next-generation capture (FENGC): precision targeted single-molecule profiling of epigenetic heterogeneity, chromatin dynamics, and genetic variation*. 2022.11.08.515732.

Zhou, M., Paul, A.-L., and Ferl, R.J. (2017) *Data for characterization of SALK_084889, a T-DNA insertion line of Arabidopsis thaliana*. *Data in Brief*, **13**, 253–258.

Zhou, M., Sng, N.J., LeFrois, C.E., Paul, A.-L., and Ferl, R.J. (2019) *Epigenomics in an extraterrestrial environment: organ-specific alteration of DNA methylation and gene expression elicited by spaceflight in Arabidopsis thaliana*. *BMC Genomics*, **20**, 205.

Supporting Information

Table S1. Information of 108 capture targets.

Table S2. Oligos used in this study.

Table S3. Filtered HiFi reads on target and targets detected.

Table S4. Number of filtered HiFi reads aligned to 108 targets.

Figure S1. Correlation between numbers of filtered HiFi reads aligned to targets and the GC content of target regions in each sample.

Figure S2. Percentage of full-length reads and truncated reads mapped in seven selected target regions.

Figure S3. FENGC results for *ABCB17*.

Figure S4. FENGC results for AT4G22217.

Figure S5. Correlation between proportions of methylated cytosines in different sequence contexts within the same molecule in the captured region of *PDF1.1*.

Figure S6. Correlation between proportions of methylated cytosines in different sequence contexts within the same molecule in the captured region of *EMO1* (AT1G27565).

Figure S7. Proportion of methylated CG, CHG and CHH sites within the same molecule in the captured region of *EMO1* (AT1G27565).

Figure S8. Correlation between proportions of methylated cytosines in different sequence contexts within the same molecule in the captured region of *EMO2* (AT5G52710).

Figure S9. Proportion of methylated CG, CHG and CHH sites within the same molecule in the captured region of *EMO2* (AT5G52710).

Figure S10. FENGC results for AT4G04990.

Figure S11. Correlation between proportions of methylated cytosines in different sequence contexts within the same molecule in the captured region of AT4G04990.

Figure S12. Proportion of methylated CG, CHG and CHH sites within the same molecule in the captured region of AT4G04990.

Figure S13. Relative transcription levels of *EMO1*, *EMO2* or AT4G04990 in their mutants, respectively.

Figure S14. Characterization of root growth in mutants of *EMO1*, *EMO2* or AT4G04990.

Figure S15. Root gravitropism in mutants of *EMO1*, *EMO2* or AT4G04990.

Figure Legends

Figure 1. Application of flap-enabled next-generation capture (FENGC) in root samples of *Arabidopsis* experiencing spaceflight.

(A) Percentage of filtered HiFi reads on target for all 108 targets. Reads with more than three consecutive methylated CHH sites were removed. GCR, Ground Col Roots; FCR, Flight Col Roots; GER, Ground control *elp2-5* Roots; FER, Flight *elp2-5* Roots. (B) Percentage of targets detected by at least 1 filtered HiFi read or at least 10 filtered HiFi reads. (C) Correlation between numbers of total filtered HiFi reads of all samples aligned to targets and the GC content of target regions. Log transformation of reads number was done by $\log_2$(read number +1). R-squared value and *p* value of logarithmic regression analysis are shown. (D) Correlation coefficients between biological replicates of FENGC and between FENGC and WGBS for average cytosine methylation levels in seven example targets.

Figure 2. FENGC results for *CML46.*

(A) Genic region of *CML46*. The target region is indicated by brown rectangle (target ID: AT5G39670-1 in S1 Table). A MYB-like binding element is indicated by green brick. The transcription start site is indicated by arrow. (B) Expression levels of *CML46* in Ground control Col-0 Roots (GCR), Flight Col-0 Roots (FCR), Ground control *elp2-5* Roots (GER) and Flight *elp2-5* Roots (FER). Gene expression is indicated by average count per million mapped reads (CPM) in RNA-seq reported by Paul et al. 2021. Lowercase letters indicate significant differences between samples (FDR < 0.05 in DESeq2). (C) Average CG methylation level within the target region. The relative position of MYB-like binding element shown in (A) is indicated by green brick. The region indicated by dashed frame shows significant differences of CG methylation level between FCR and GCR (One-way ANOVA with post-hoc Tukey HSD test; *, $p < 0.05$). (D) Distribution of proportion of methylated CG sites per molecule in filtered, full-length HiFi reads aligned

to the target region. The box indicates the upper and lower quartiles of the data set. The whiskers extend to the largest or the smallest data point that is within 1.5 times the interquartile range. The data points of mPPM are represented by dots. The line and “x” in the box indicate median and mean, respectively. The significant differences of methylation proportion are shown (Kruskal-Wallis test; *, $p < 0.05$; **, $p < 0.01$). (E) Heatmaps showing CG methylation of single molecules. Red indicates two consecutively methylated cytosines, black indicates two consecutively unmethylated cytosines, and gray indicates borders between methylated and unmethylated cytosines. The reads from the four biological replicates (Table S4) were combined to generate heatmaps for each sample. The relative position of MYB-like binding element shown in (A) and (C) is indicated by green brick. The region used for the CG methylation level comparison in (C) is indicated by dashed frame. Around 6.9% reads in GCR and 12% reads in FCR containing at least 2 consecutively methylated CG sites in both areas flanking the MYB-like binding element are labeled by blue bricks. One-way ANOVA with post-hoc Tukey HSD test was performed for pairwise comparisons of percentage of reads with this signature. FER vs FCR, $p < 0.01$.

Figure 3. FENGC results for *PDF1.1.*

(A) Genic region of *PDF1.1*. The target region is indicated by brown rectangle (target ID: AT1G75830-1 in Table S1). A MeJA-responsive element is indicated by green brick. The transcription start site is indicated by the arrow. (B) Expression levels of *PDF1.1* that are presented in the same way of Figure 2B. (C) Average CG, CHG or CHH methylation levels over all sequenced molecules of the target region. The relative position of MeJA-responsive element shown in (A) is indicated by green brick. The significant differences of methylation levels between samples for CHG and CHH sites in the target region are shown. One-way ANOVA with post-hoc Tukey HSD test; *, $p < 0.05$; **, $p < 0.01$; ***, $p < 0.001$. Black arrows indicate DmCs detected in WGBS using the threshold of methylation difference > 0.2 and FDR < 0.01. Arrows of solid line and dot line indicate DmCs of GER vs GCR and FER vs GER, respectively. (D) Distribution of proportion of methylated CG, CHG or CHH sites per molecule in filtered full-length

HiFi reads aligned to the target region. The significant differences of methylation proportion are shown (Kruskal-Wallis test; *, $p < 0.05$; **, $p < 0.01$; ***, $p < 0.001$). (E) Heatmaps showing the cytosine methylation in single molecules. Reads from the four biological replicates (Table S4) were combined to generate heatmaps for each sample. If the number of combined reads exceeded 1,000, 1,000 reads were randomly selected and plotted. The three heatmap panels show the patterns of methylation at CG, CHG, and CHH sites (vertical white lines) as indicated at bottom along the same DNA molecule in each row. The color legend is the same as that in Figure 2E. Reads were hierarchically clustered using Kendall's Tau based on CG methylation. The relative position of MeJA-responsive element shown in (A) is indicated by green brick. A footprint (blue ovals) with consecutive protection against methylation of the first 2 CG sites in the area flanking the MeJA-responsive element is present in 8.4%, 18.0%, 39.4% and 44.0% molecules in GCR, FCR, GER and FER, respectively. One-way ANOVA with post-hoc Tukey HSD test was performed for pairwise comparisons of percentage of reads with this footprint. FCR vs GCR, $p < 0.05$; GER vs GCR, $p < 0.001$; FER vs FCR, $p < 0.001$.

Figure 4. DNA methylation within same molecules in the target region of *PDF1.1.*

(A) Proportion of methylated CG, CHG and CHH sites within the same molecule in the captured region of AT1G75830. There are 120, 1009, 345 and 1310 full-length reads covering all CG, CHG and CHH sites in this region (target ID: AT1G75830-1 in Table S1), which are mapped for GCR, FCR, GER and FER samples, respectively. Ochre, gold and dark green dots indicate CG, CHG and CHH methylation proportions, respectively, in the same column, each representing one read. (B) Comparisons of methylation proportions per molecule in reads with a footprint and in all reads in the captured region of AT1G75830. CHG and CHH methylation in GCR, FCR, GER and FER samples are plotted, respectively. The footprint is defined as the first 2 CG sites in this target region that are both unmethylated. The significant differences of methylation proportion are shown (Kruskal-Wallis test; *, $p < 0.05$; **, $p < 0.01$; ***, $p < 0.001$).

Figure 5. FENGC results for *EMO1*.

(A) Genic region of *EMO1*. The target region is indicated by brown rectangle (target ID: AT1G27565-1 in Table S1). An anaerobic-responsive element (ARE) is indicated by green brick. The transcription start site (TSS) is indicated by arrow. (B) Expression levels of *EMO1* that are presented in the same way of Figure 2B. (C) Average CG, CHG or CHH methylation levels in cytosines within the target region. The relative position of ARE and TSS shown in (A) are indicated by green brick and arrow, respectively. The significant differences of CG methylation level between samples in the target region are shown, in which the first CG site is omitted. One-way ANOVA with post-hoc Tukey HSD test; *, $p < 0.05$; ***, $p < 0.001$. Black arrows indicate DmCs of FER vs GER detected in WGBS using the threshold of methylation difference > 0.2 and FDR < 0.01. (D) Distribution of proportion of methylated CG, CHG or CHH sites per molecule in filtered full-length HiFi reads aligned to the target region. The significant differences of methylation proportion are shown (Kruskal-Wallis test; *, $p < 0.05$). (E) Heatmaps showing the cytosine methylation in single molecules. The heatmap panels and color legend are the same as that in Figure 3E. Reads were hierarchically clustered using Euclidean distance based on CG methylation. The percentages of reads without methylated CG sites and reads with at least 9 consecutive unmethylated CG sites at the 3' end are shown on the left and right side of the CG panel, respectively. One-way ANOVA with post-hoc Tukey HSD test was performed for pairwise comparisons. For percentages of reads without methylated CG sites, FER vs GER, $p < 0.05$; GER vs GCR, $p < 0.001$; FER vs FCR, $p < 0.01$. For percentages of reads with at least 9 consecutive unmethylated CG sites at the 3' end, FCR vs GCR, $p < 0.01$; GER vs GCR, $p < 0.01$.

Figure 6. FENGC results for *EMO2*.

(A) Genic region of *EMO2*. The target region is indicated by brown rectangle (target ID: AT5G52710 in Table S1). Two MeJA-responsive elements are indicated by green bricks. The transcription start site (TSS) is indicated by arrow. (B) Expression levels of *EMO2* that are presented in the same way of Figure 2B. (C) Average CG, CHG or CHH

methylation levels in cytosines within the target region. The relative position of MeJA-responsive elements shown in (A) are indicated by green bricks. The significant differences of CG and CHG methylation levels between samples in the target region are shown. One-way ANOVA with post-hoc Tukey HSD test; **, $p < 0.01$; ***, $p < 0.001$. Black arrows indicate the DmCs detected in WGBS using the threshold of methylation difference > 0.2 and FDR < 0.01. Arrows with solid line, triangle, round end, and dot line indicate DmCs of GER vs GCR, FER vs FCR, FCR vs GCR, and FER vs GER, respectively. (D) Distribution of proportion of methylated CG, CHG or CHH sites per molecule in filtered full-length HiFi reads aligned to the target region. The significant differences of methylation proportion are shown (Kruskal-Wallis test; ***, $p < 0.001$). (E) Heatmaps showing the cytosine methylation in single molecules. The reads clustering, heatmap panels and color legend are the same as that in Figure 5E.

Figure 7. Enhanced root growth in mutants of *EMO1* or *EMO2*.

(A) 7-day old seedlings of Col-0, *emo1-1*, *emo1-2*, *emo2-1*, and *emo2-2*. Scale bars indicate 10 mm. (B) Primary root length of 4-day old and 7-day old seedlings for each line. (C) Average root growth rate (mm per day) from day-0 to day-4, and from day-4 to day-7. Student's t test, *, $p < 0.05$; **, $p < 0.01$; ***, $p < 0.001$. Data ± SD, n = 33 to 55 for each condition.

Table 1. Comparison of multiplexed, targeted DNA sequencing methods in plants. Light gray indicates advantages and dark gray indicates disadvantages.

Method	Custom design liberty	Read length	Example of sequencing depth	Example of on-target read % in plant genome	Example of target number	Cost	Adaptation in DNA methylation detection
Multiplexed PCR	**limited by low complexity of sequences**	**Short (e.g., < 200 bp)** (Onda *et al.*, 2018)	**1,000x** (Onda *et al.*, 2018)	**50.9 %** (Onda *et al.*, 2018)	**443 markers** (Onda *et al.*, 2018)	**low**	**no**

Probe hybridization-based	**limited by commercial panels and costly design**	**short/long (e.g., 3.5 kb)** (Giolai *et al.*, 2017)	**55x** (Giolai *et al.*, 2017)	**52.9%** (Hill *et al.*, 2019)	**190 genes** (Hill *et al.*, 2019)	**high due to modified probes**	**no**
CRISPR-based	**limited by PAM sites and cleavage efficiency**	**short/long (e.g. 8 kb)** (López-Girona *et al.*, 2020)	**~200x** (López-Girona *et al.*, 2020)	**3.04%** (López-Girona *et al.*, 2020)	**1 gene** (López-Girona *et al.*, 2020)	**high due to RNA oligos and specific proteins**	**no**
FENGC	**cleavage for any site**	**short/long (e.g., > 500 bp)**	**10-5,000x**	**~90%**	**102 genic regions**	**low**	**long-read EM-seq**

821

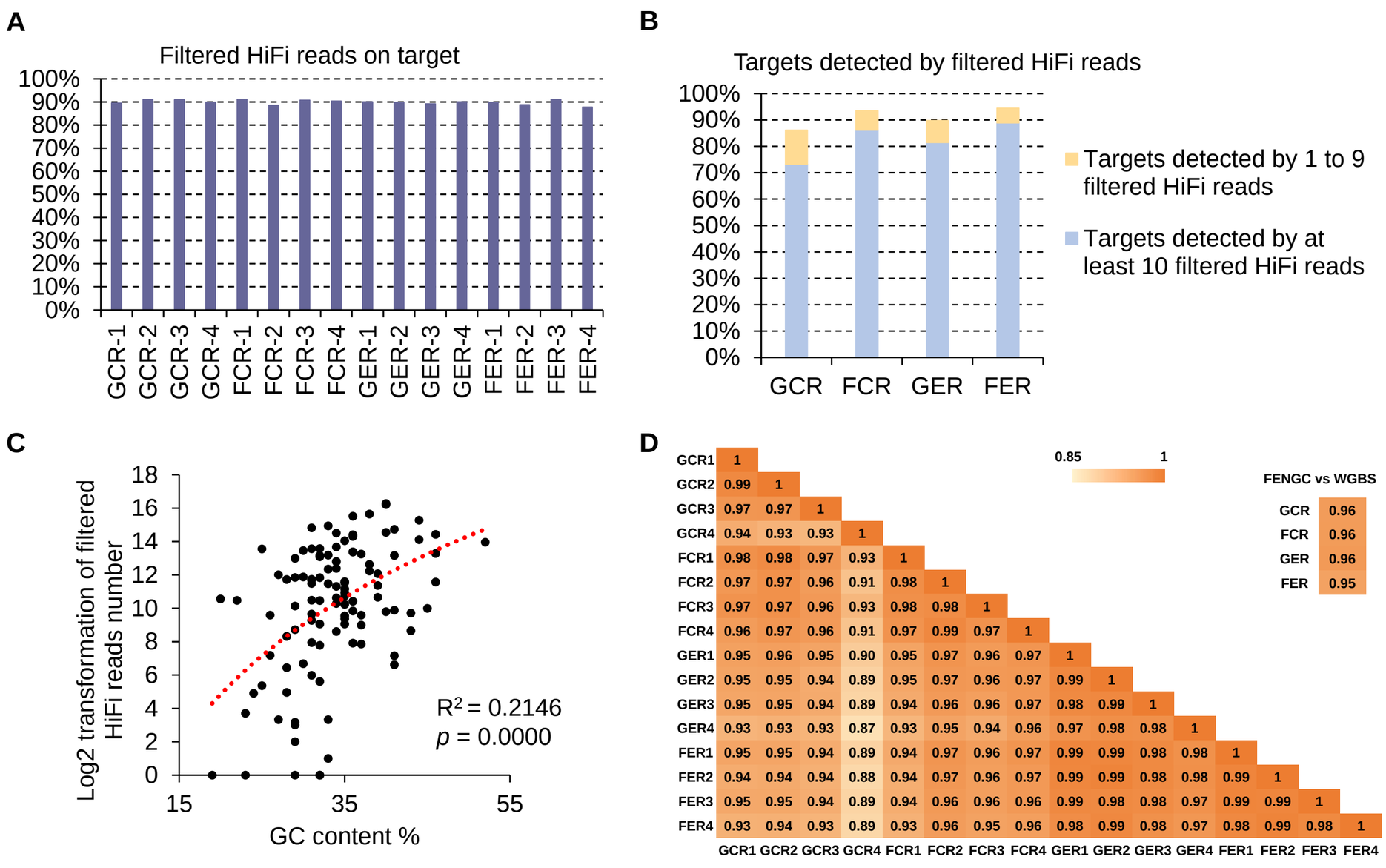
A
Filtered HiFi reads on target
100%
90%
80%
70%
60%
50%
40%
30%
20%
10%
0%
GCR-1
GCR-2
GCR-3
GCR-4
FCR-1
FCR-2
FCR-3
FCR-4
GER-1
GER-2
GER-3
GER-4
FER-1
FER-2
FER-3
FER-4
B
Targets detected by filtered HiFi reads
GCR
FCR
GER
FER
Targets detected by 1 to 9 filtered HiFi reads
Targets detected by at least 10 filtered HiFi reads
C
Log2 transformation of filtered HiFi reads number
GC content %
R2 = 0.2146
p = 0.0000
D
0.85
1
FENGC vs WGBS
GCR 0.96
FCR 0.96
GER 0.96
FER 0.95
GCR1 1
GCR2 0.99 1
GCR3 0.97 0.97 1
GCR4 0.94 0.93 0.93 1
FCR1 0.98 0.98 0.97 0.93 1
FCR2 0.97 0.97 0.96 0.91 0.98 1
FCR3 0.97 0.97 0.96 0.93 0.98 0.98 1
FCR4 0.96 0.97 0.96 0.91 0.97 0.99 0.97 1
GER1 0.95 0.96 0.95 0.90 0.95 0.97 0.96 0.97 1
GER2 0.95 0.95 0.94 0.89 0.95 0.97 0.96 0.97 0.99 1
GER3 0.95 0.95 0.94 0.89 0.94 0.96 0.96 0.97 0.98 0.99 1
GER4 0.93 0.93 0.93 0.87 0.93 0.95 0.94 0.96 0.97 0.98 0.98 1
FER1 0.95 0.95 0.94 0.89 0.94 0.97 0.96 0.97 0.99 0.99 0.98 0.98 1
FER2 0.94 0.94 0.94 0.88 0.94 0.97 0.96 0.97 0.99 0.99 0.98 0.98 0.99 1
FER3 0.95 0.95 0.94 0.89 0.94 0.96 0.96 0.96 0.99 0.98 0.98 0.97 0.99 0.99 1
FER4 0.93 0.94 0.93 0.89 0.93 0.96 0.95 0.96 0.98 0.99 0.98 0.97 0.98 0.99 0.98 1
GCR1 GCR2 GCR3 GCR4 FCR1 FCR2 FCR3 FCR4 GER1 GER2 GER3 GER4 FER1 FER2 FER3 FER4

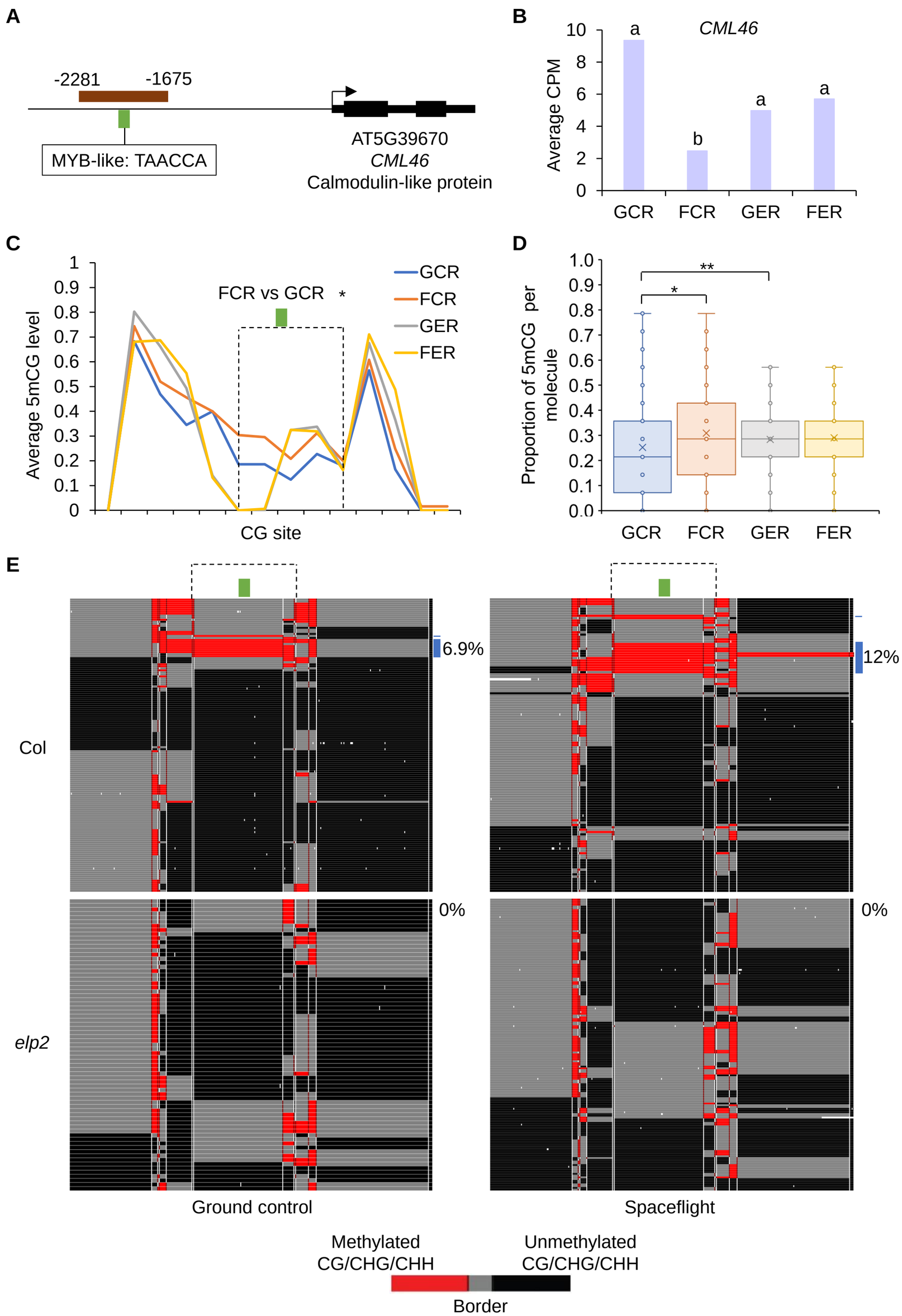
A
-2281
-1675
MYB-like: TAACCA
AT5G39670
CML46
Calmodulin-like protein
B
CML46
Average CPM
a
b
a
a
GCR
FCR
GER
FER
C
FCR vs GCR *
Average 5mCG level
CG site
GCR
FCR
GER
FER
D
Proportion of 5mCG per molecule
**
*
GCR
FCR
GER
FER
E
Col
elp2
6.9%
0%
12%
0%
Ground control
Spaceflight
Methylated CG/CHG/CHH
Unmethylated CG/CHG/CHH
Border

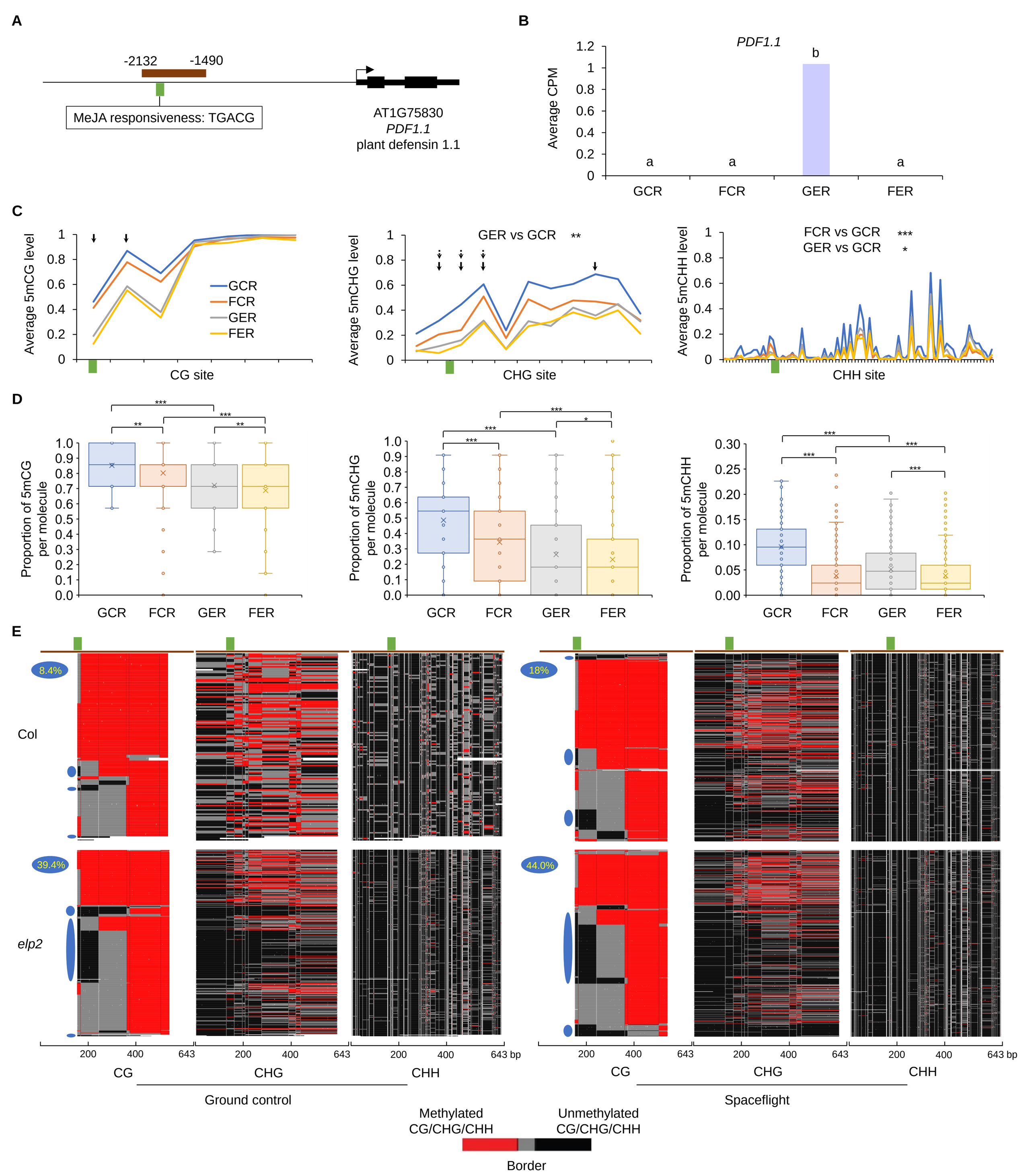
A
-2132
-1490
MeJA responsiveness: TGACG
AT1G75830
PDF1.1
plant defensin 1.1
B
PDF1.1
Average CPM
a
a
b
a
GCR
FCR
GER
FER
C
Average 5mCG level
GCR
FCR
GER
FER
CG site
Average 5mCHG level
GER vs GCR **
CHG site
Average 5mCHH level
FCR vs GCR ***
GER vs GCR *
CHH site
D
Proportion of 5mCG per molecule
Proportion of 5mCHG per molecule
Proportion of 5mCHH per molecule
GCR
FCR
GER
FER
E
Col
elp2
8.4%
39.4%
18%
44.0%
200
400
643
643 bp
CG
CHG
CHH
Ground control
Spaceflight
Methylated CG/CHG/CHH
Unmethylated CG/CHG/CHH
Border

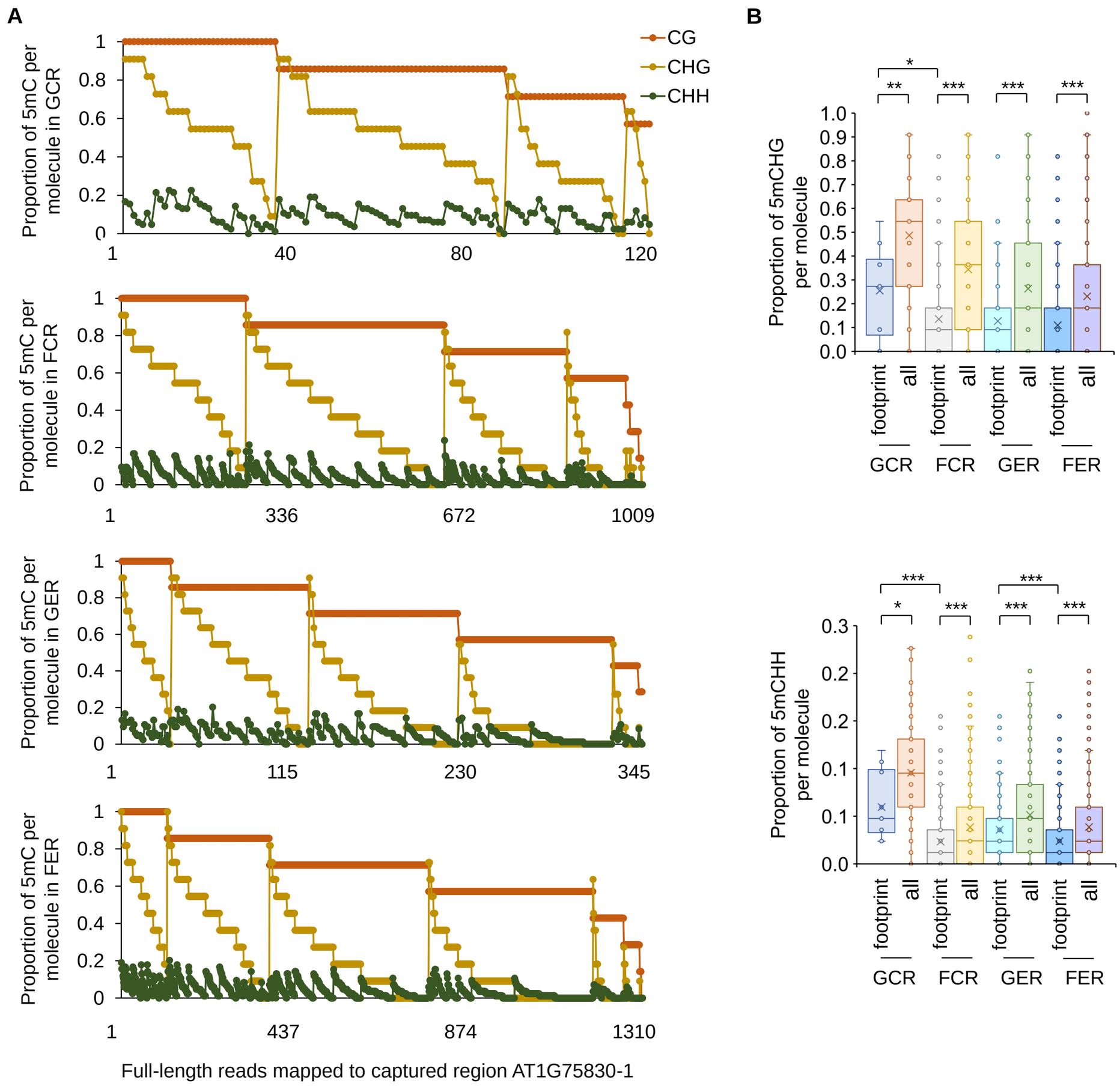
A
B
CG
CHG
CHH
Proportion of 5mC per molecule in GCR
Proportion of 5mC per molecule in FCR
Proportion of 5mC per molecule in GER
Proportion of 5mC per molecule in FER
1
0.8
0.6
0.4
0.2
0
1
40
80
120
336
672
1009
115
230
345
437
874
1310
Full-length reads mapped to captured region AT1G75830-1
Proportion of 5mCHG per molecule
Proportion of 5mCHH per molecule
1.0
0.9
0.8
0.7
0.6
0.5
0.4
0.3
0.2
0.1
0.0
*
**
***
footprint
all
GCR
FCR
GER
FER

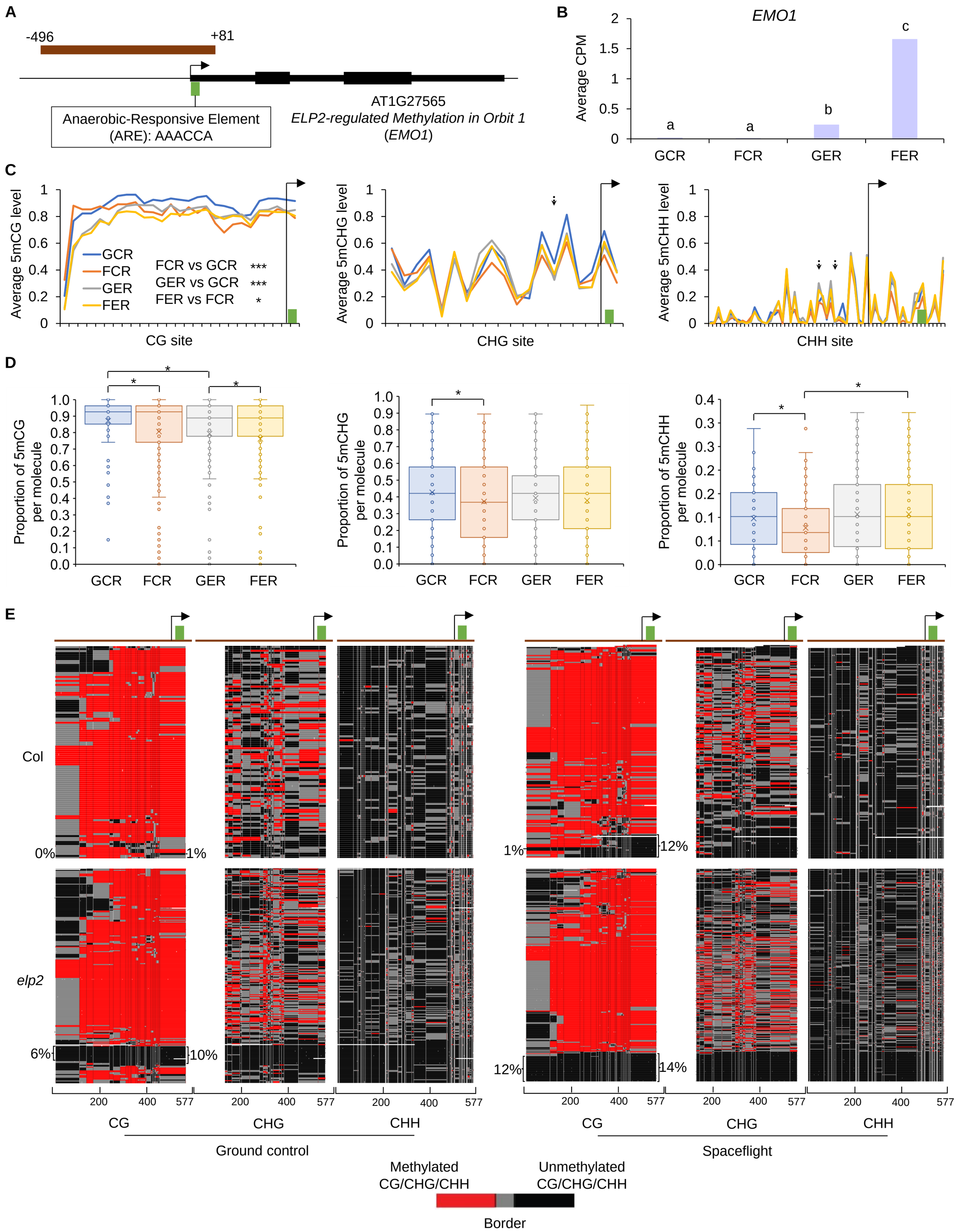
A
-496
+81
Anaerobic-Responsive Element (ARE): AAACCA
AT1G27565
ELP2-regulated Methylation in Orbit 1 (EMO1)
B
EMO1
Average CPM
GCR
FCR
GER
FER
C
Average 5mCG level
Average 5mCHG level
Average 5mCHH level
CG site
CHG site
CHH site
FCR vs GCR ***
GER vs GCR ***
FER vs FCR *
D
Proportion of 5mCG per molecule
Proportion of 5mCHG per molecule
Proportion of 5mCHH per molecule
E
Col
elp2
0%
1%
6%
10%
12%
14%
CG
CHG
CHH
Ground control
Spaceflight
Methylated CG/CHG/CHH
Unmethylated CG/CHG/CHH
Border

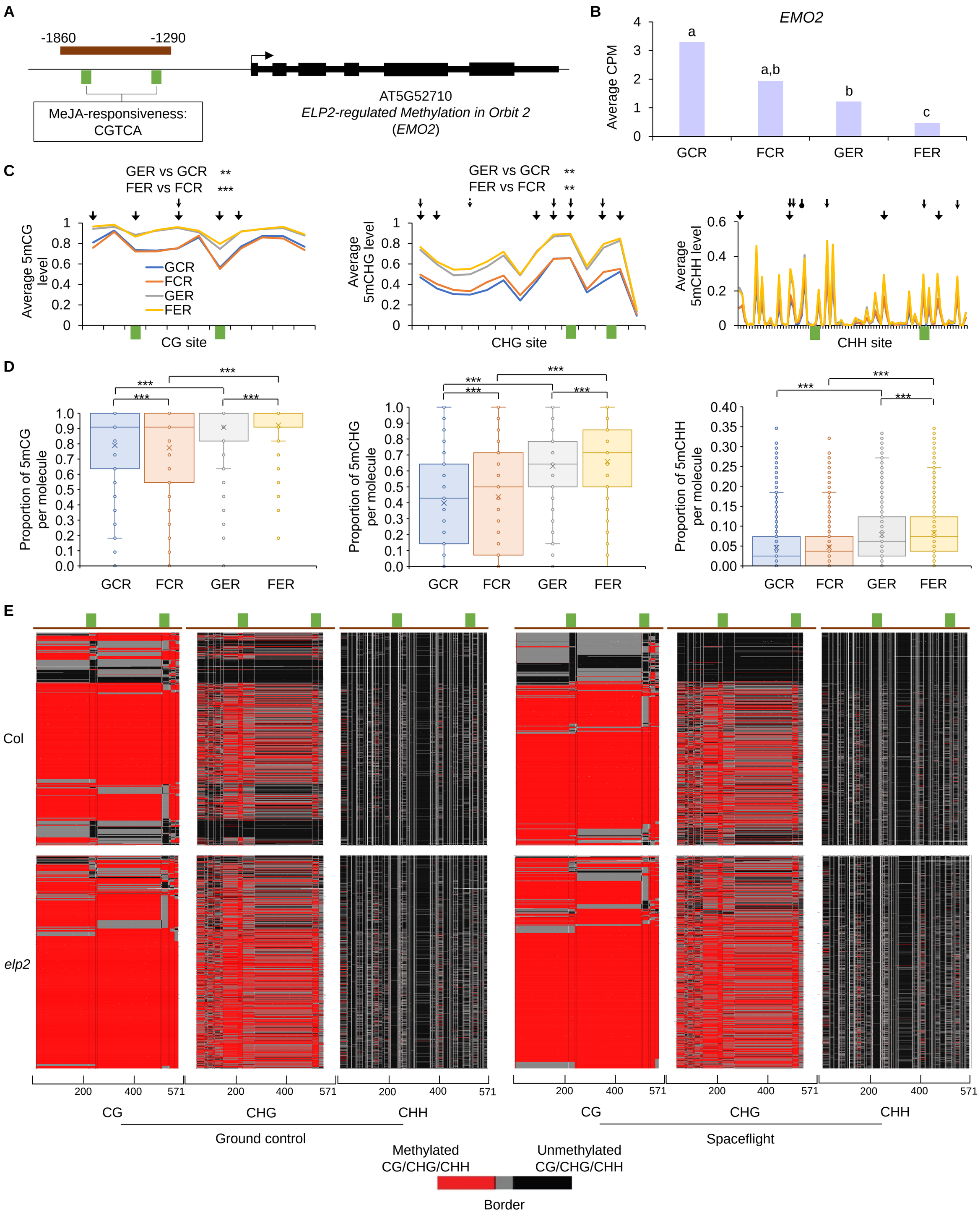
A
-1860
-1290
MeJA-responsiveness:
CGTCA
AT5G52710
ELP2-regulated Methylation in Orbit 2
(EMO2)
B
EMO2
Average CPM
a
a,b
b
c
GCR
FCR
GER
FER
C
GER vs GCR **
FER vs FCR ***
Average 5mCG level
GCR
FCR
GER
FER
CG site
GER vs GCR **
FER vs FCR **
Average 5mCHG level
CHG site
Average 5mCHH level
CHH site
D
Proportion of 5mCG per molecule
Proportion of 5mCHG per molecule
Proportion of 5mCHH per molecule
***
E
Col
elp2
200
400
571
CG
CHG
CHH
Ground control
Spaceflight
Methylated CG/CHG/CHH
Unmethylated CG/CHG/CHH
Border

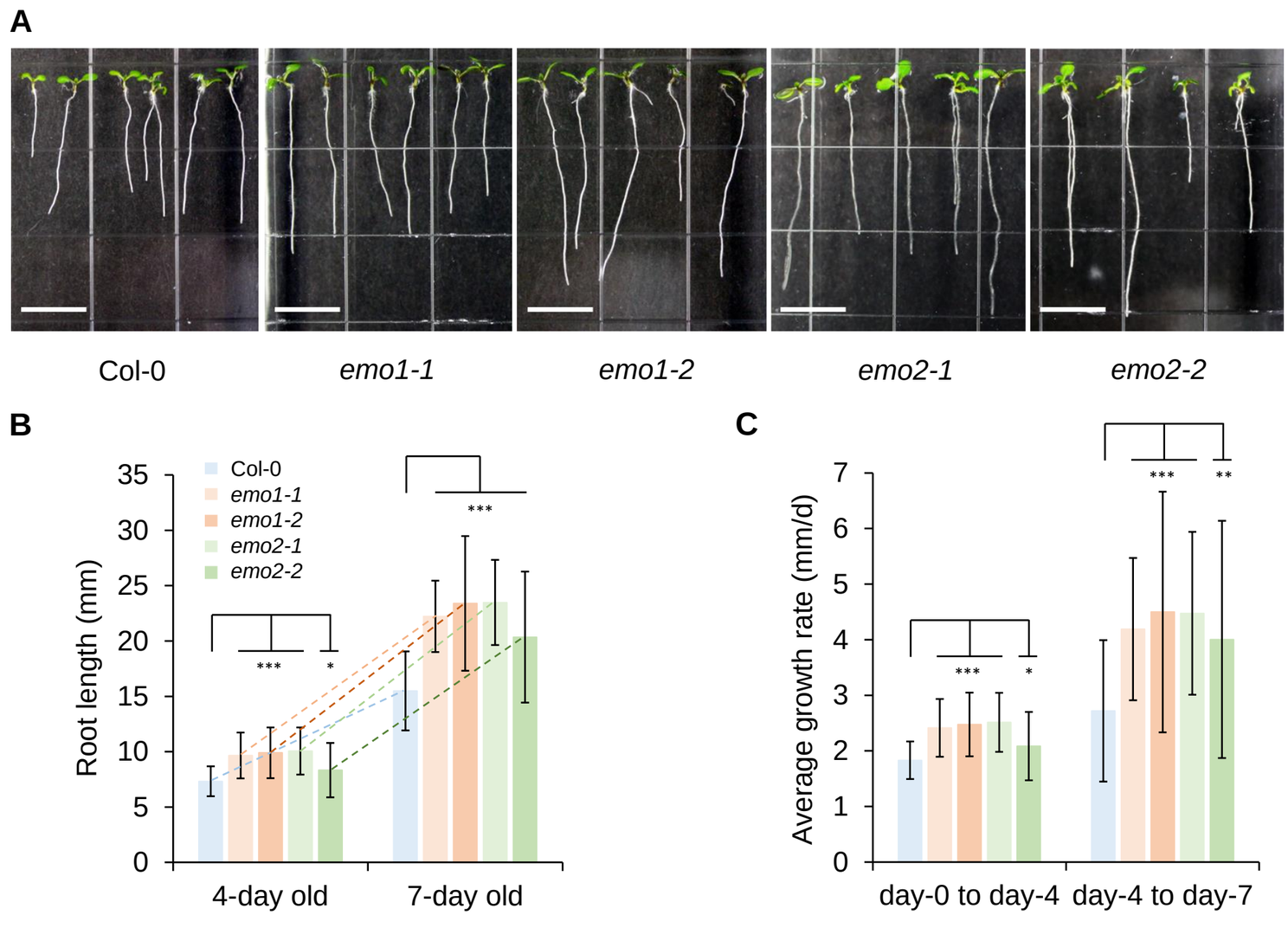
A
Col-0
emo1-1
emo1-2
emo2-1
emo2-2
B
Root length (mm)
35
30
25
20
15
10
5
0
Col-0
emo1-1
emo1-2
emo2-1
emo2-2
***
*
***
4-day old
7-day old
C
Average growth rate (mm/d)
7
6
5
4
3
2
1
0
***
*
***
**
day-0 to day-4
day-4 to day-7